RESEARCH ARTICLE | JANUARY 05 2024

Development of the 174 GHz collective Thomson scattering diagnostics at Wendelstein 7-X
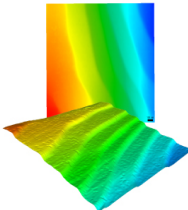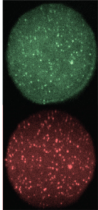
S. Ponomarenko ✉ ; D. Moseev ; T. Stange ; L. Krier ; P. Stordiau ; H. Braune; G. Gantenbein ;
J. Jelonnek ; A. Kuleshov ; H. P. Laqua ; C. Lechte ; S. Marsen ; S. K. Nielsen ;
J. W. Oosterbeek ; B. Plaum ; R. Ragona ; J. Rasmussen ; T. Ruess ; M. Salewski ;
M. Thumm ; J. Zimmermann ; W7-X Team

Check for updates

CrossMark

View Online

Export Citation

AIP Publishing

Development of the 174 GHz collective Thomson scattering diagnostics at Wendelstein 7-X

S. Ponomarenko,[1,a] (ID)   D. Moseev,[1] (ID)   T. Stange,[1] (ID)   L. Krier,[1,2] (ID)   P. Stordiau,[3] (ID)   H. Braune,[1]
G. Gantenbein,[2] (ID)   J. Jelonnek,[2] (ID)   A. Kuleshov,[4] (ID)   H. P. Laqua,[1] (ID)   C. Lechte,[5] (ID)   S. Marsen,[1] (ID)
S. K. Nielsen,[6] (ID)   J. W. Oosterbeek,[1] (ID)   B. Plaum,[5] (ID)   R. Ragona,[6] (ID)   J. Rasmussen,[6] (ID)   T. Ruess,[2] (ID)
M. Salewski,[6] (ID)   M. Thumm,[2] (ID)   J. Zimmermann,[1] (ID)   and W7-X Team[b]

AFFILIATIONS

[1] Max Planck Institute for Plasma Physics, D-17491 Greifswald, Germany
[2] IHM, Karlsruhe Institute of Technology, D-76131 Karlsruhe, Germany
[3] Eindhoven University of Technology, 5612 AZ Eindhoven, Netherlands
[4] O.Ya. Usikov Institute for Radiophysics and Electronics, NASU, 61085 Kharkiv, Ukraine
[5] IGVP, University of Stuttgart, D-70569 Stuttgart, Germany
[6] Department of Physics, Technical University of Denmark, DK-2800 Lyngby, Denmark

[a] Author to whom correspondence should be addressed: sergiy.ponomarenko@ipp.mpg.de
[b] See T. S. Pedersen *et al.*, Nucl. Fusion **62**, 042022 (2022) for the full list of W7-X team members.

ABSTRACT

In this paper, we present the design and commissioning results of the upgraded collective Thomson scattering diagnostic at the Wendelstein 7-X stellarator. The diagnostic has a new radiometer designed to operate between the second and third harmonics of the electron cyclotron emission from the plasma at 171–177 GHz, where the emission background has a minimum and is of order 10–100 eV. It allows us to receive the scattered electromagnetic field with a significantly improved signal-to-noise ratio and extends the set of possible scattering geometries compared to the case of the original instrument operated at 140 GHz. The elements of the diagnostic are a narrowband notch filter and a frequency stabilized probing gyrotron that will allow measuring scattered radiation spectra very close to the probing frequency. Here, we characterize the microwave components applied to the radiometer and demonstrate the performance of the complete system that was achieved during the latest experimental campaign, OP2.1.

I. INTRODUCTION

The principle of Collective Thomson Scattering (CTS) diagnostics is based on the scattering of electromagnetic radiation at collective microscopic fluctuations in a fusion plasma. During the measurements, a probing microwave beam is directed into the plasma vessel, where a CTS receiver antenna picks up the scattered radiation. Depending on the probing beam frequency, plasma parameters, and scattering geometry, the scattering can be either coherent (collective) or incoherent. The distinction between these cases is commonly defined by the parameter α introduced by Salpeter.[1] Collective scattering occurs when $\alpha > 1$. In the case of the used scattering configurations of the upgraded CTS diagnostic, the Salpeter parameter $\alpha > 3$ for typical temperatures $T_e \approx 2.3$ keV and densities $n_e \approx 6 \times 10^{19}$ of the viewed plasmas at the Wendelstein 7-X (W7-X) stellarator. When the plasma parameters are close to the goal operation of the stellarator, such as $n_e = 2.4 \times 10^{20}$ and $T_e = 2$ keV, the criteria is $\alpha = 6.5$. The outcome of the measurements is a power spectral density (PSD) function of the scattered radiation. A dedicated scattering model evaluates the corresponding plasma parameters based on this function, such as ion temperature, plasma drift velocities, fast ion velocity distribution function, or plasma composition.[2–4] Such CTS measurements have, for example, been shown at ASDEX Upgrade[5,6] or LHD.[7] A CTS diagnostic will also be installed at ITER.[8,9]

15 January 2024 07:04:52

The plasma fluctuations are resolved along the axis defined by the difference vector $\boldsymbol{k}_d = \boldsymbol{k}_s - \boldsymbol{k}_i$, where $\boldsymbol{k}_i$ is the incident wave vector and $\boldsymbol{k}_s$ is the scattered wave vector. The scattering geometry is defined by $\boldsymbol{k}_i$ and $\boldsymbol{k}_s$, but also by the angle between the local magnetic field $\boldsymbol{B}$ and $\boldsymbol{k}_d$. In addition, the scattered radiation depends on the radiation patterns of the probe and receiver antenna systems since the CTS signal originates from the volume at which both microwave beams overlap. Moreover, electromagnetic waves propagating in plasmas experience refraction, which can cause certain difficulties in defining the actual overlap volume, depending on plasma parameters.[2,10]

At the W7-X stellarator, the CTS diagnostic utilizes the available infrastructure of the electron cyclotron resonance heating (ECRH) facility.[11,12] Particularly, one of the total twelve beamlines of the quasi-optical ECRH transmission system and a corresponding probing beam gyrotron are used for CTS purposes. The CTS measurements are possible with one of two receiving antennas mounted in the triangular and bean-shaped cross sections of module 1 of the stellarator.[11] The antennas are switched manually, depending on the research program. The transmission line is optimized for low attenuation, which contributes to the high sensitivity of the CTS receiver. The beamline joints of the antenna systems are located in the plasma vessel, and a microwave radiometer is mounted outside of the torus hall. In the future, the diagnostic will be equipped with its own transmission line due to the upcoming upgrade of the ECRH plant.[12] The general architecture of the diagnostic can be found in the earlier publications.[13,14]

The first experimental findings of the CTS diagnostic at W7-X,[13] operated at 140 GHz, demonstrated the capability of ion temperature measurements. However, the assessment of other plasma quantities was complicated, mainly because of the poor signal-to-noise ratio (SNR), since the scattering occurred in the frequency range of the electron cyclotron emission (ECE).[13] A strong ECE background in the order of several keV makes the detection of fast ion signatures in the scattering spectra nearly impossible.[10] Moreover, unattainable plasma regions located behind the resonance layer and strong refraction at high plasma density restrict the capabilities of the diagnostic when operated at 140 GHz.

In order to mitigate the influence of the high ECE background and to increase the sensitivity of the diagnostic, it was proposed to shift the probing frequency to the range between the second and third ECE harmonics, where the cyclotron emission is greatly reduced.[15] The CTS diagnostics at ASDEX Upgrade and LHD operate between the first and second harmonics, and the one at ITER is below the first. The point-by-point considerations of the possible frequency range[10] were performed by taking into account other important aspects too, such as microwave reflections from the vacuum windows and the wave refraction in the plasma volume. Based on this, a probing beam frequency of 174 GHz was selected for future CTS measurements.[16,17] With the 174 GHz gyrotron at W7-X, operation between the second and third harmonics is now possible. The key features of the upgraded instrument are high SNR, the application of a narrowband notch filter compared to the existing 140-GHz diagnostic, and the use of a frequency stabilized gyrotron that makes such an approach feasible. Moreover, the new system allows the measurements to be performed everywhere along the minor radius in both cross-sections. In this paper, we present the design of the upgraded 174 GHz CTS diagnostic at the W7-X stellarator and discuss the commissioning results obtained during the latest operational program. The performance of the upgraded system is compared to that of its predecessor, which operated at 140 GHz.

The paper is organized as follows: In Sec. II, we present the design of the 174 GHz heterodyne microwave radiometer and discuss the performance of the main components as well as the overall noise characteristics of the receiver. Activities related to the commissioning of the diagnostic are discussed in Sec. III. In Sec. IV, we summarize the results of test measurements of the ECE background performed with the help of the upgraded CTS radiometer at 171–177 GHz. The conclusions to this work are given in Sec. V.

II. DESIGN OF THE 174 GHz CTS RADIOMETER

The 174 GHz CTS diagnostic is built around a sensitive heterodyne radiometer with a single intermediate-frequency (IF) stage. The schematics of the radiometer is shown in Fig. 1. The front-end of the receiver uses the WR-6 (D-band) standard. Although we plan for measurements beyond the recommended frequency limit of the D-band waveguide, this can be performed without the risk of exciting high-order modes in the waveguide. This is because the next waveguide mode has a cutoff frequency close to 181.6 GHz. The electromagnetic radiation propagates in the form of a Gaussian beam from the receiver antenna to the radiometer input. The conversion of the beam to the TE_{10} rectangular waveguide mode occurs in a matching optics unit (MOU). The MOU consists of an off-axis parabolic mirror, a flat mirror, and an antenna. The original 140 GHz CTS diagnostic used a corrugated horn, which is not suitable for 174 GHz due to distortions in the radiation pattern.[18] Therefore, it is replaced by a new dual-band smooth-walled horn antenna optimized for both 140 and 174 GHz. After the MOU, the radiation can be guided with the help of a waveguide switch (Hughes) either to the 140 GHz or to the 174 GHz receiver front-end. There is no need to enable simultaneous operation of both systems since a single probing gyrotron is used. Switching between the operating frequencies requires a ramping of the magnetic field of the gyrotron that takes up to one day. In order to reduce the signal attenuation at 174 GHz, the waveguide switch connects the antenna to the receiver front-end via a straight arm. The switch is well-matched with the transmission line and has low insertion loss (IL < 1.5 dB) in the frequency range from 137 to 180 GHz.

The transmission line between the MOU and the down converter includes protection against gyrotron stray radiation, namely a notch filter and a voltage-controlled variable attenuator. A cascade of bandpass filters suppresses the image frequencies of the heterodyne system and protects the receiver from the radiation of heating gyrotrons. A full D-band Faraday isolator (Elva-1, https://elva-1.com), which has high isolation (better than −25 dB) and low insertion loss (IL = 3 dB), is used in the front-end to reduce the effect of reflected waves. Before entering the mixer, the received scattered radiation is amplified by a broadband monolithic microwave integrated circuit (MMIC) amplifier.[19] After the down conversion, the IF signal is boosted by a low-noise amplifier and passes through the low pass filter. Due to safety reasons, the radiometer is placed in a closed metal case, shielding it from any stray radiation coming from the quasi-optical transmission line. At the back-end of the radiometer, a fast 8-bit analog-to-digital converter (ADC) (PXIe-5186, National
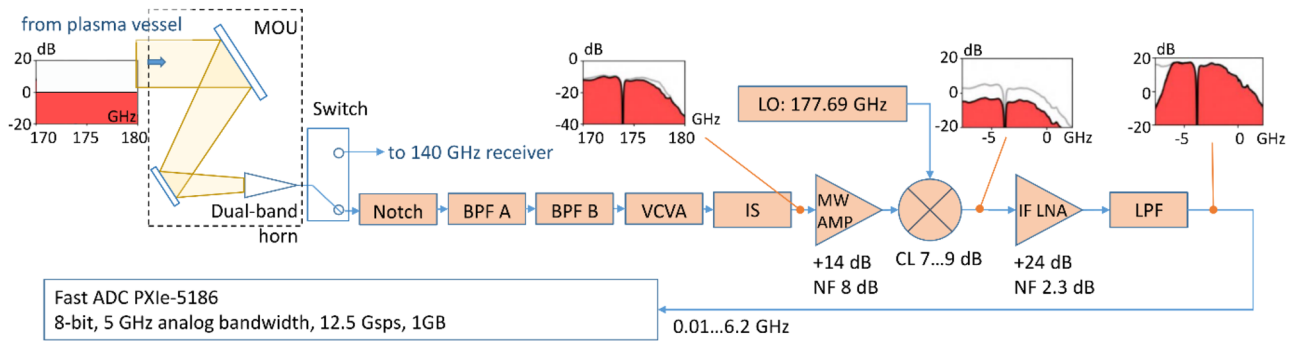
FIG. 1. The schematics of 174 GHz CTS radiometer: MOU – matching optics unit, BPF – bandpass filter, VCVA – voltage-controlled variable attenuator, IS – microwave isolator, MW AMP – broadband MMIC amplifier, LO – local oscillator, LNA – low noise amplifier, LPF – low pass filter, ADC – analog to digital converter.

Instruments) is used to process the detected scattered signals.[14] During the measurements at 174 GHz, the acquisition system runs at a maximal sample rate of 12.5 Gsps.

Below, in this section, the results of the measurements are presented, and the performance of the microwave components applied to the upgraded CTS radiometer is discussed. The scattering parameters S_{11} and S_{21} were measured in dB with the help of a network analyzer, PNA N5222B (Keysight), and the frequency extension modules (VDI). The parameters S_{11} and S_{21} define the return loss and insertion loss of a component as RL = $-S_{11}$ and IL = $-S_{21}$, respectively.

A. Adjustment of the notch filter

A key element of the CTS radiometer is a notch filter used to protect the receiver from the powerful stray radiation coming from the probing gyrotron. The filter should have a rejection strong enough to protect the microwave mixer and ensure that the total microwave power seen by the mixer stays below 0 dBm. An ideal notch filter should have a narrow rejection band for measuring a scattering spectrum near the probing frequency. In practice, the rejection bandwidth of the filter is constrained by the frequency drifts of the probing gyrotron[2] and is typically 200–500 MHz when measured at the maximal attenuation level.[2,20] The rejection bandwidth must be significantly extended when the measurements occur in the presence of many gyrotrons operated at similar frequencies. That is the case for the 140 GHz CTS diagnostic at W7-X. The ECRH gyrotrons at W7-X have a nominal frequency range of 140 to 140.5 GHz. Therefore, the notch filters of the 140 GHz CTS diagnostic are tuned to the center frequency of 140.14 GHz and have a 3-dB rejection bandwidth of about 900 MHz. Moreover, the filters have an additional stopband at 137 GHz to damp the parasitic radiation that can be generated by one of the 140 GHz gyrotrons.

The CTS diagnostics operating between the second and third harmonics of ECE are not affected by stray radiation coming from the heating gyrotrons because of the use of two band-pass filters with more than 40 dB damping each outside of the transmission band, particularly at 140 GHz. This means that the frequency of the probing gyrotron can be stabilized to make the application of a narrowband notch filter feasible. Moreover, one can reduce the

requirement for maximal damping from 160 dB to around 50–60 dB, which is enough for a single 500–800 kW tube.[21] As a result, one can potentially analyze CTS spectra very close to the probe frequency. This is important for more accurate inference of the ion temperature, detecting spectral features that appeared due to plasma composition, and turbulence.[22]

The notch filter is tuned according to the operational characteristics of the probing gyrotron at 174 GHz. A millisecond after the startup, the frequency of the free-running gyrotron is 173.95 GHz, but due to the thermal expansion of the cavity and electron beam space charge neutralization, the frequency drifts further during the pulse. Eventually, the shift is about 30 MHz at the end of a single pulse lasting 10 ms. For this reason, the center frequency of the rejection band is adjusted to 173.92 GHz. The frequency response of the tuned filter is shown in Fig. 2. The settings provide an attenuation of up to −60 dB in the frequency range from 173.91 to 173.93 GHz and a 3 dB rejection bandwidth of 460 MHz. The frequency of the probing gyrotron is stabilized using a Phase-Locked Loop (PLL), which is discussed in Sec. III.

B. Bandpass filters and protection against stray radiation

Usually, a microwave bandpass filter (BPF) is used in a heterodyne system to suppress image frequencies and define the operating frequency range. This is also the case for the 140 GHz radiometer, which contains a BPF-06/135–145 filter from Elva-1. However, in the case of the 174 GHz system, the BPF serves as an element of passive protection against the stray radiation coming from the heating gyrotrons operated at 140 GHz. The reason is the utilization of D-band waveguides (the cutoff frequency of the TE_{10} mode is 90.8 GHz) and the absolute transparency of the 174 GHz notch filter at 140 GHz (see Fig. 2). Therefore, a cascade of two BPFs is used to satisfy this requirement.

The applied cascade consists of the filters BPF-06/170-180 (Elva-1) and BPF-02E/171-177 (Elmika). The measured scattering parameters S_{11} and S_{21} of the components are shown in Fig. 3. Both filters have similar insertion losses of 2 to 3 dB. The full damping of the cascade is about 6 dB at 171–177 GHz. At the same time, the cascade attenuates signals by more than 120 dB in the frequency range below 165 GHz. The total reflections S_{11} are less than −10
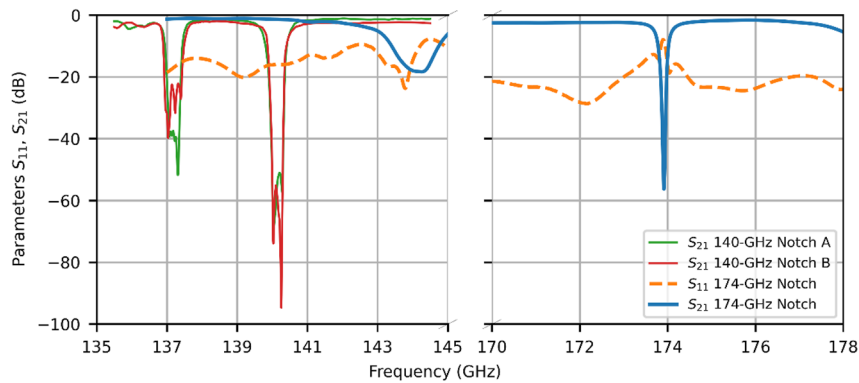
FIG. 2. The scattering parameters S_{11}, S_{21} of the notch filters measured in the corresponding frequency ranges of the 140 and 174 GHz CTS diagnostics. The transmission characteristics of the 174-GHz notch filter are also measured at 137–145 GHz.

dB at 170–176.8 GHz, thus contributing to a good matching of the transmission line.

The CTS receiver contains a voltage-controlled variable attenuator (VCVA), which prevents excessive microwave power from reaching the mixer during the switching on/off of the gyrotron due to the frequency shift of its oscillation. Moreover, a narrowband notch filter requires additional protection for the microwave mixer before the emission frequency is stabilized at a value covered by the rejection band of the notch filter. Consequently, the oscillation frequency chirps are compared to the "cold" state by hundreds of MHz.[2,23]

In the 174 GHz radiometer, a voltage-controlled variable attenuator VCVA-06/170-180 (Elva-1) is used. Its parameters are summarized in Fig. 4. The attenuator is controlled by a bias current and can be closed in less than 0.1 ms after receiving a control signal. The attenuator stays closed during the gyrotron switching on/off. During the CTS acquisition intervals, the VCVA is set in a state that is selected for each particular discharge to prevent damage to the receiver. The VCVA has an almost flat frequency response and a minimum attenuation of 2 dB in the range from 137 to 176 GHz.
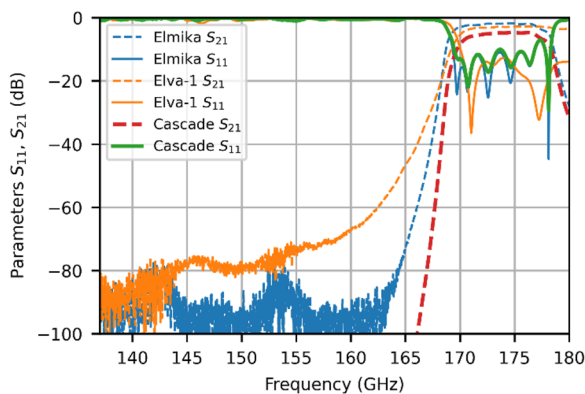
The low reflection $S_{11} < -10$ dB is provided by the device in the open state at 171.3–177.12 GHz, which corresponds to the planned operating band of the upgraded CTS diagnostic. The maximum damping of the attenuator exceeds 60 dB.

C. Downconverter unit and the IF stage

The converter unit of the 174-GHz CTS radiometer is built around a single-IF architecture and uses a high-side injection. In order to boost the CTS signal and reduce the total noise figure of the system, a D-band broadband MMIC amplifier (Elva-1) is placed before the downconverter. In addition, the amplifier serves as a buffer, providing auxiliary isolation between the downconverter and the waveguide components. The device operates in linear mode with a gain of 14 dB in the D-band up to 180 GHz. The Y-factor method is used to define the noise figure of the amplifier. Therefore, a value of 8 dB is obtained from the measurements carried out with the help of a noise source, ISSN-06 (Elva-1). The noise source is pre-calibrated in the frequency range from 172 to 180 GHz and has an excess noise ratio of 15 dB. The results of these measurements are shown in Fig. 5.

The IF-stage contains a fixed-frequency local oscillator, FOM-06/178/172-184 (Elva-1), which pumps a balanced mixer, BM-06/172/172-184 (Elva-1), at 177.69 GHz. The conversion losses (CL) of the diode are examined with the help of a signal generator MG3694C (Anritsu) and the 12th harmonic frequency extender WR5.1140–220 GHz (VDI) that delivers about 0 dBm at 170–180 GHz. The strength of the IF signal is measured by using the spectrum analyzer FSP (Rohde & Schwarz). The conversion losses of the mixer are measured in the range of 7–9 dB. At the same time, the level of IF harmonics does not exceed −35 dB in the considered frequency range.

At the next step, the IF signal is amplified by a 24-dB low-noise amplifier (Kuhne electronics) placed after the mixer to maximize the dynamic range of the digitizer. The LNA has a flat gain response and a noise figure of 2.3 dB in the IF frequency range from 1 to 8 GHz. In the IF range from 1.5 to 4.5 GHz, the input port of the amplifier is well matched (RL > 14 dB) with the transmission line, while the same condition is valid for the output port when the IF < 6 GHz. However, the wave reflections appear at the input port in the range from 5 to 6.5 GHz, where RL is up to 6 dB. After the
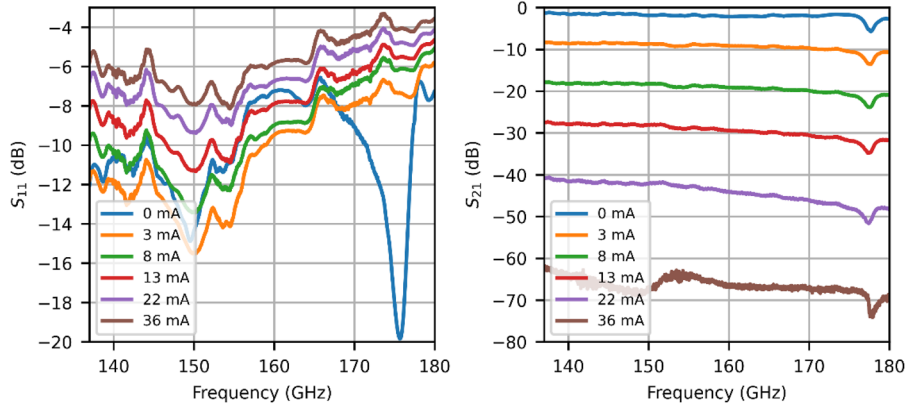

FIG. 3. Scattering coefficients S_{11} and S_{21} measured for the bandpass filters applied in the 174 GHz CTS receiver.

FIG. 4. The scattering parameters S_{11} and S_{21} demonstrated by the VCVA at different control currents.

LNA, the IF signal passes through the low-pass filter (M.E.L., IL < 0.5 dB, RL > 12 dB) and enters the fast ADC (RL > 10 dB). The LPF has a cutoff frequency of 6.2 GHz. Therefore, the ADC can process the converted signal with a sampling rate of 12.5 GSps. In practice, the CTS radiation is extremely weak, and the expected input microwave power of the radiometer is under the limit at which the gain compression or the digital saturation effects can be observed. The main interferer of the CTS signal is the gyrotron stray radiation, which can cause both of these problems when the gyrotron frequency appears outside of the maximal rejection region of the notch filter. Therefore, in the upgraded system, the PLL circuit is used to stabilize the gyrotron frequency in the range of maximal attenuation and to support the linear operation of the receiver. According to the transmission characteristics of the notch filter (Fig. 2) and the noise figure of the IF-stage components (Fig. 5), a significant decrease in the signal-to-noise ratio of the radiometer is expected above 176.5 GHz. However, this is not a significant concern since these frequencies are far from the center frequency of the predicted scattering spectrum.[10]
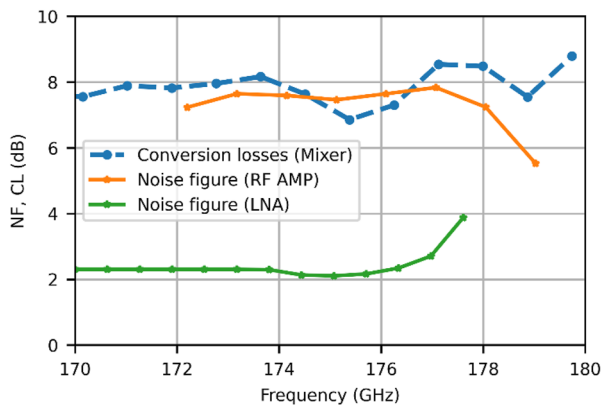

FIG. 5. The noise figures (NF) of the amplifiers and the conversion losses (CL) of the mixer applied in the IF-stage of the 174 GHz CTS radiometer.

D. Noise figure characterization

The total noise factor F_t of the radiometer is estimated with the help of the Friis formula for cascaded two-port devices[24] from the known parameters of each component placed in between the MOU antenna and the digitizer. In the case of a 174 GHz radiometer, the total noise factor (disregarding the impact of the ADC) is defined as follows:

$$F_t = F_{RF}F_{PA} + F_{RF}(F_{mix}F_{LNA} - 1)$$
$$/G_{PA} + F_{RF}F_{mix}(F_{LPF} - 1)/G_{PA}G_{LNA}, \qquad (1)$$

where F_{RF}, F_{PA}, F_{mix}, F_{LNA}, and F_{LPF} are the noise factors of the main elements, namely the transmission line, the MMIC amplifier, the mixer, the IF low-noise amplifier, and the low pass filter. The transmission line includes the waveguide components placed in between the MOU and the microwave amplifier. The coefficients G_n define the power amplification of the corresponding element n. The noise factor of a passive element n equals its own insertion loss and also defines the gain factor $G_n = 1/F_n$. All the parameters in the noise factor formula are on a linear scale. The first term, $F_{RF}F_{PA}$, provides the main contribution to the radiometer's intrinsic noise and depends on the transmission losses in the waveguide components and the noise factor of the MMIC amplifier. Therefore, there is room for improvement in the total noise factor by using another advanced amplifier with a better noise figure. The total attenuation of the transmission line from the distributed measurements for the parameter S_{21} of each component is defined. Note that the parameter S^C_{21} of a cascade C, which consists of the two 2-port elements A and B, is defined on the linear scale as $S^C_{21} = S^B_{21}S^A_{21}/(1 - S^B_{11}S^A_{22})$. The parameter $S^n_{22} = S^n_{11}$ is for a passive 2-port element n. However, when the product $S^A_{22}S^B_{11}$ is negligible, the total transmission coefficient S^C_{21} can be defined in dB as a simple sum of $20\log_{10}S^A_{21}$ and $20\log_{10}S^B_{21}$. The expected error of the total transmission does not exceed 3 dB when the product $S_{22}S_{11}$ is less than 0.3.

In Fig. 6, the characteristics of both the new 174 GHz receiver and the existing 140 GHz system are compared in terms of the total transmission coefficient S_{21} as well as the total noise figure. The noise figure of the used ADC NF$_{ADC}$ takes values from 24 to 30 dB, and its
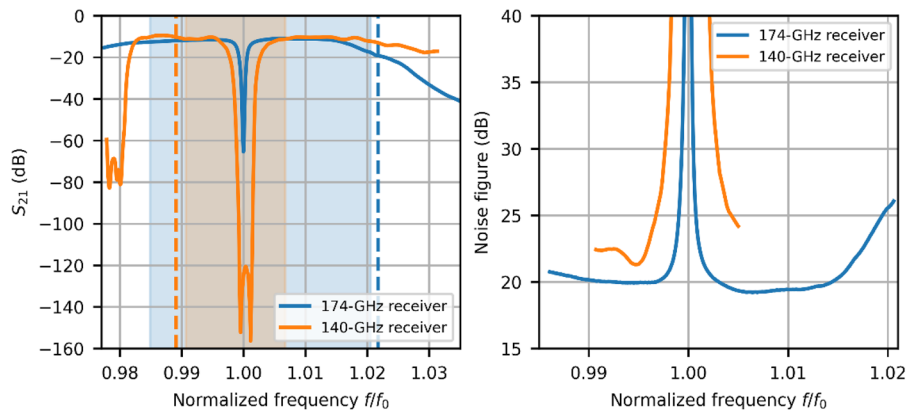
FIG. 6. (Left) The total insertion losses are calculated for the transmission lines of both 140- and 174 GHz receivers from the results of distributed measurements: dashed lines represent the frequencies of the corresponding LO, and shaded areas represent the operating frequency ranges of the receivers. (Right) The noise figure of the two CTS receivers (disregarding the impact of the ADC). The frequency axis is normalized by the center frequency of the corresponding notch filters, f_0 = 140.1 GHz and f_0 = 173.92 GHz.

contribution to the overall noise performance of the 174-GHz system reduces to about 1 dB due to the presence of both amplifiers. The available −3 dB band of the transmission line lies within the range of 170.38–176.93 GHz. Except at frequencies within the stopband of the notch filters, both receivers have comparable insertion loss. However, in the 174 GHz system, the use of the MMIC amplifier before the down-converting circuit allows for mitigating the effect of the noise from the subsequent components. The equivalent noise temperature T_e of the receiver calculated from the noise factor as T_e = 293 K(F_t − 1) is 2–3 eV for the upgraded system and 4–7 eV for the 140-GHz radiometer. The upgraded radiometer has almost flat noise characteristics in the frequency ranges located below and above (up to 176.53 GHz) the rejection band. This feature allows useful data to be obtained on both the red- and blue-shifted sides of the scattering spectra. However, the most important point is the reduction in noise figure in the region close to the probing frequency, which is achieved by using the narrow band notch filter.

III. COMMISSIONING THE CTS RADIOMETER

The commissioning of the 174 GHz CTS radiometer includes an alignment of the quasi-optical transmission line, a calibration of the receiver, and a frequency tuning of the probing gyrotron. The correct alignment prevents the loss of the beam on the way from the gyrotron to the plasma vessel and back to the receiver.[13] Furthermore, it is important for allowing accurate identification of the spatial origin of the detected CTS signal. The tuning of the probing frequency is critical in the case of using a narrow band notch filter. Therefore, it is necessary to use a stabilization system for locking the gyrotron operation at the frequency that guarantees the strongest damping at the rejection band of the filter.

A. Microwave alignment of the quasi-optical transmission line

The alignment procedure of the CTS diagnostic entails an adjustment of the quasi-optical transmission lines for both the probing and the receiving beams. Infrared-thermography is used to detect the pattern of the Gaussian beam propagating in the quasi-optical transmission line.[13] An infrared camera is used to capture the thermal footprint of the beam on a thin microwave absorber fixed to a certain mirror or window. If the footprint appears away from the intended central position, the preceding movable mirror is adjusted. First, the beam pattern of the probing beam, which propagates in the transmission line B1,[13,14] is aligned in order to hit the center of the entrance vacuum window of the plasma vessel. The gyrotron itself serves as a source of the test radiation in this case. The quasi-optical transmission line F1[13,14] between the vessel and the CTS receiver is examined in the same manner at the second step. However, a compact low-power source is used instead of the gyrotron. In the case of thermographic measurements, it is important to supply enough microwave power to heat the target in a short period. This allows us to mitigate distortions in the footprint due to the heat diffusion effect. According to estimations, a microwave power of 1 W is required to make the measurements for the F1 line. Unfortunately, in the given frequency range, such a magnitude is excessive for modern solid-state electronics. Therefore, a watt-level compact clinotron oscillator developed by IRE NASU (Ukraine) is used. The oscillator allows measurements at frequencies up to 175 GHz.[25] The clinotron is connected to a dual-band horn antenna to feed the receiving line. Therefore, all necessary radiation footprints are collected, and the quasi-optical transmission line is aligned for operation at 174 GHz. An example footprint of the aligned receiver beam propagating through the torus window is shown in Fig. 7.

B. Calibration of the CTS radiometer

A hot/cold source procedure is used to calibrate the CTS radiometer. Losses in the quasi-optical transmission line B1 between the MOU and the plasma vessel are not incorporated in the calibration for practical reasons. Despite that, the performed calibration is assumed to be absolute since the total damping in the excluded line does not exceed 3%.[11,26] The black-body source is a piece of *Eccosorb* placed at room temperature T_{amb} and at the temperature of liquid
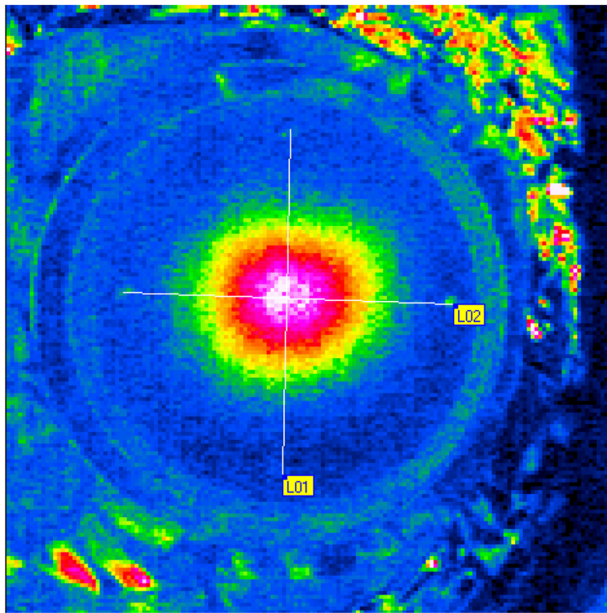
15 January 2024 07:04:52

FIG. 7. Thermal footprint of the microwave beam captured at the vacuum window of the plasma vessel in the receiver beamline F1.

nitrogen T_{LN2}. The field of view of the receiver antenna is switched to calibration mode by changing the position of the steerable flat mirror, which is located in the MOU in front of the horn antenna. The calibration setup is demonstrated in Fig. 8. The antenna views the cold body, placed in an isolated chamber, through a circular aperture. The shutter with the hot body attached above moves horizontally and periodically closes the aperture, thus changing the view from one source to the other. The pairs of spectra are collected during 20 ms time intervals and in immediate succession to minimize

random observation error. Finally, a function is received that is averaged over the total calibration time. This function maps the obtained power spectral density to the source temperature across the considered frequency range. In practice, the measurements are obtained for a total duration of several hours in order to achieve sufficient statistics.

In addition to obtaining a calibration curve, the results can be used to define the equivalent noise temperature T_{rec} of the receiver. According to the Y-factor method,[27] the temperature T_{rec} is found as $T_{rec} = \frac{T_{amb} - Y T_{LN2}}{Y - 1}$, where $Y = \frac{P_{amb}}{P_{LN2}}$ is the ratio of power levels detected by the receiver during the hot/cold source measurements. The radiometer noise temperature derived from the calibration data is shown in Fig. 8. The instrument response exhibits small ripples, which could appear due to the imperfect isolation of the receiver transmission line and cables. Nevertheless, the upgraded CTS receiver has a reduced noise level compared to its 140 GHz predecessor. Moreover, the experimental data also confirms the calculations for the noise temperature discussed in Sec. II D.

C. Frequency stabilization of the probing gyrotron

A gyrotron is a vacuum electron device that operates using the effects of electron cyclotron radiation.[28] In the gyrotron, electrons interact with a high-order transverse electric TE mode of an overmoded cylindrical cavity. The oscillating frequency f and the interaction efficiency depend on the chosen TE mode and the static axial magnetic field B in the cylindrical cavity. The frequency f roughly scales with the magnetic field as f [GHz] = 28·B/γ [T], where γ is the relativistic Lorentz factor.

At W7-X, the CTS diagnostic uses one of the ECRH gyrotrons (Thales TH1507 prototype "Maquette" at place B1). The gyrotron was designed for nominal operation in the $TE_{28,8}$ mode, delivering an output power of about 1 MW at 140.1 GHz. For the CTS diagnostic, theoretical investigations were carried out to operate the 140-GHz W7-X gyrotron in the 170–180 GHz frequency range.[16] The most suitable operating mode is the $TE_{34,10}$ mode at 173.9 GHz,
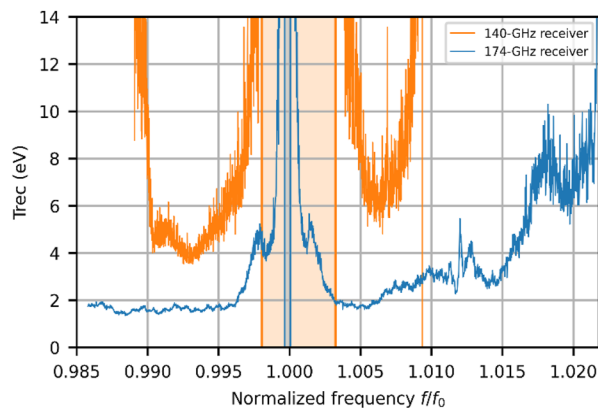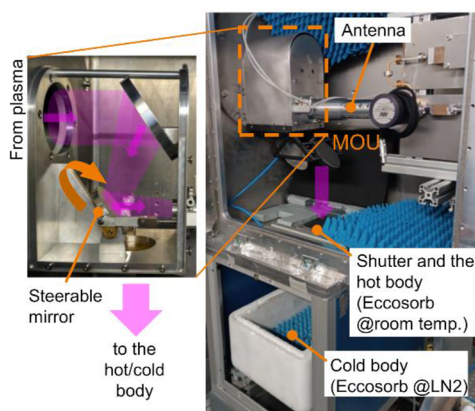
FIG. 8. (Left) A view at the calibration setup installed in the receiver box. Inset: the propagation of a Gaussian beam in the MOU box. (Right) The equivalent noise temperature of both receivers operated at 174 and 140 GHz. The frequency axis is normalized by the corresponding center frequency of the notch filters, namely f_0 = 140.1 GHz and f_0 = 173.92 GHz.

which requires a static magnetic field B of 7 T. For the experiments, the gyrotron is installed in a cryogen-free 7.1 T magnet.[29] The tube demonstrates stable performance in the $TE_{34,10}$ mode for pulse lengths up to 10 ms. An output power of about 300 kW is measured. Moreover, an additional operation region can be observed at 171 GHz in $TE_{33,10}$ mode, where an output power of 500 kW was measured. Nevertheless, this mode is less preferable for operation because of the higher reflectivity of the gyrotron output window at this frequency.

The gyrotron cavity experiences a certain thermal expansion during the start of operation because of the ohmic heating of the cavity. Additionally, the neutralization of the electron beam during the start of the gyrotron must be considered. Consequently, the frequency of a free-running gyrotron drifts.[2,13,23] In the case of the probing gyrotron operating at 174 GHz, the frequency drifts more than 30 MHz during a pulse of 10 ms length [Fig. 9(a)]. The radiation propagating in the plasma has a very small absorption in this frequency range. Therefore, a strong probing signal reflected from the walls and picked up by the CTS antenna can appear outside of the rejection band of the notch filter. This will saturate or even damage the receiver. To mitigate the effect of thermal expansion and to keep the probing radiation close to the frequency of maximal rejection, a frequency stabilization system for the probing gyrotron was developed.[30] The system uses the PLL and controls the accelerating voltage U_{acc} of the gyrotron with a diode-type Magnetron Injection Gun (MIG) to compensate for the frequency drift. The accelerating voltage is changed via the body power supply. With the PLL system, the gyrotron frequency is stabilized within 3 ms after the gyrotron startup. In particular, it implies that the VCVA has to be fully closed during the first 5 ms of a gyrotron pulse to protect the receiver from the strong stray radiation in the frequency range outside the rejection band. This measure also discards any oscillations of other parasitic TE modes that could be excited during the startup phase. The accurate tuning of the gyrotron parameters, such as the static magnetic field in the cavity and the accelerating voltage U_{acc}, along

with the proper adjustment of the stabilization circuit, allows us to run the gyrotron at 173.928 GHz, the frequency that corresponds to the maximal attenuation in the notch filter [see Fig. 9(d)]. The exact frequency is defined from the experiment [Fig. 9(b)], where the oscillating frequency shifts through the rejection region. Finally, the PLL control is configured to hold the desired frequency during a pulse sequence required for the CTS measurements. Both Figs. 9(c) and 9(d) demonstrate that the gyrotron frequency locks at two different values during the acquisition pulses that lasted 3 ms and that are repeated every 140 ms. The spectrograms shown in Fig. 9 are composed of the mean spectra averaged over the acquisition.

IV. ECE MEASUREMENTS AT 174 GHz

The verification of the CTS radiometer was carried out during plasma operation at W7-X. The practical goal was to measure the radiation temperature of the ECE at 170–180 GHz and to compare the results with the available measurements from the ECE Michelson interferometer (MI)[31,32] and the ECE radiometers.[33,34]

The CTS radiometer collected ECE signals within intervals lasting 5 ms, which had a period of 200 ms. The first sample was measured before the onset of plasma heating, i.e., without plasma, to evaluate the background response. Therefore, the useful signal is the difference between subsequent pulses and the background. The typical ECE spectrum averaged over an acquisition interval is shown in Fig. 10 for a representative discharge No. 20230314.52. The measured values of power spectral density were converted to eV by using the absolute calibration data discussed in Sec. III B. The measured ECE level gradually increases with frequency and reaches almost 75 eV at 175 GHz. The data from MI show a similar value at the same frequency and confirm a small increase in the ECE level between the second and third ECE harmonics. Note that the MI is not absolutely calibrated due to high attenuation in the transmission line. Therefore, a calibration obtained by the response of the interferometer to
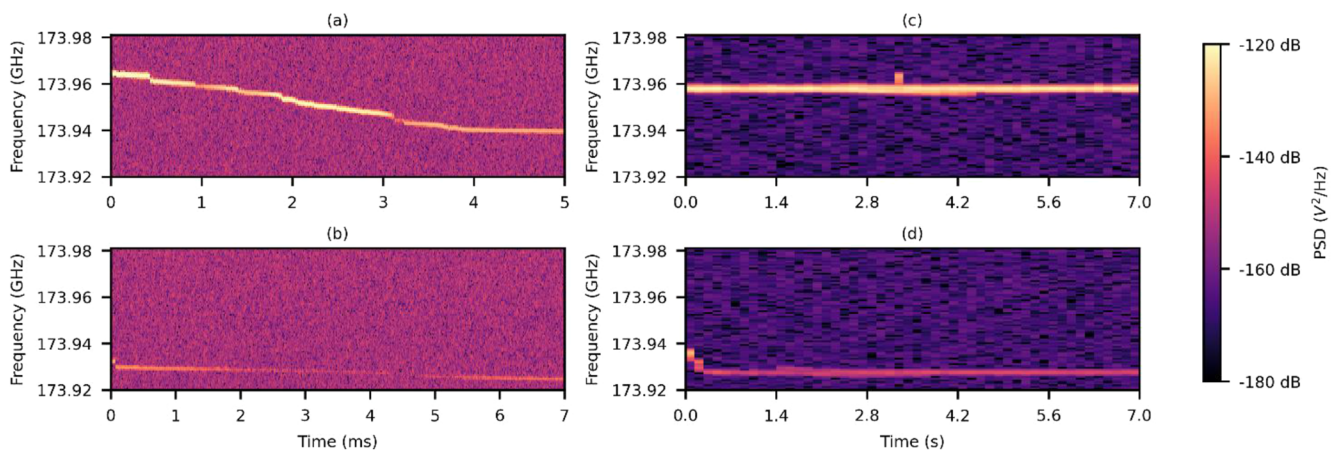
FIG. 9. (a) An example of a frequency shift, which occurs during a single pulse of the free-running probing gyrotron. (b) Attenuation of electromagnetic radiation from the partially stabilized gyrotron when the signal frequency shifts through the dip of the notch filter (between the third and fifth ms). Spectrograms of the probing gyrotron stabilized by the PLL system at: (c) 173.958 GHz (U_{acc} = 79 kV, I_m = 86.25 A), which corresponds to the high cutoff frequency edge of the rejection band; (d) 173.928 GHz (U_{acc} = 81.7 kV, I_m = 86.1 A), where the maximal rejection is provided. The current I_m of the gyrotron magnet system controls the field B in the cavity.
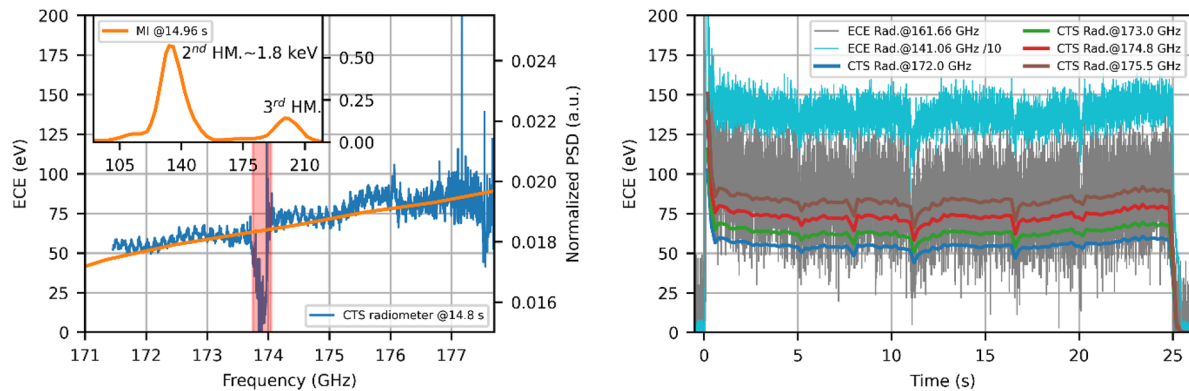
FIG. 10. (Left) An example of the ECE spectrum collected by the CTS diagnostic (thin curve) and the ECE Michelson interferometer (thick curve) during shot No. 20230314.52. (Right) Time traces of the ECE level measured during the same representative discharge by the ECE radiometers (thin curves) and the CTS diagnostic (thick curves) at different frequencies. The data from ECE radiometer channel No. 17 (141.06 GHz) have been scaled down by a factor 10.

a black body and numerically accounting for the losses in the transmission line is used. The similar signal levels demonstrated by these two diagnostics support the validity of this calibration procedure for the MI.

Time traces of the ECE signal measured at several frequencies are shown in Fig. 10. It is limited to a 300 MHz band for better SNR. The ECE level changes during the discharge because of radiation cooling caused by impurities injected by the laser blow-off system.[35,36] The changes correlate well with the data from ECE radiometers. Therefore, one can conclude that the upgraded CTS receiver definitely detected the ECE. The highest available frequency of the ECE radiometers is 161.66 GHz, which corresponds to radiometer channel No. 32. Therefore, it provides the most suitable data to use as a reference to verify our measurements. The relevant data have significant uncertainties, but even so, the mean values are in the range of 75–100 eV. Consequently, in the operation frequency range of the upgraded CTS diagnostic, the level of background emission is lower by a factor of 20–50 compared to the 1.5–1.8 keV seen at 140 GHz.

V. CONCLUSIONS

The CTS diagnostic at W7-X has been upgraded to a higher frequency for better SNR, which will allow, among others, measurements of the fast ion velocity distribution function in contrast to the pre-existing diagnostic working at 140 GHz. The improvements are achieved by changing the operating band to 171–177 GHz, a frequency range between the second and third harmonics of ECE where the emission background is almost two orders of magnitude lower.

Changes were made to a megawatt-class 140 GHz W7-X gyrotron (Thales TH1507 preprototype "Maquette") so that it can operate in the new frequency range. The modernization of the gyrotron magnet focusing system allowed gyrotron operation at 174 GHz in accordance with theoretical predictions. The frequency stabilization of the probing gyrotron using the PLL system allows us to use a very narrowband notch filter for radiometer protection. Both elements are essential features of the upgraded diagnostic, which will allow measuring scattered radiation spectra close to the

probing frequency and ensure a low ECE background for fast ion measurements.

During the commissioning phase, the quasi-optical transmission line was aligned to the new frequency band with the help of microwave thermography. The absolute calibration of the radiometer confirmed a low equivalent noise temperature of 2–3 eV, which is half that of the original 140 GHz receiver. The radiometer was tested using measurements of the ECE background at 171–177 GHz, indicating ECE levels of about 100 eV. These results are in good agreement with the data available from the ECE radiometer and Michelson interferometer. The spectra averaged over a period of 3 ms already demonstrate a better signal-to-noise ratio compared to measurements at 140 GHz, which are significantly affected by the ECE background.

AUTHOR DECLARATIONS

Conflict of Interest

The authors have no conflicts to disclose.

Author Contributions

S. Ponomarenko: Conceptualization (equal); Data curation (equal); Formal analysis (equal); Investigation (equal); Methodology (equal); Software (equal); Validation (equal); Visualization (equal); Writing – original draft (equal). **D. Moseev**: Conceptualization

(equal); Data curation (equal); Formal analysis (equal); Investigation (equal); Methodology (equal); Project administration (equal); Software (equal); Supervision (equal); Validation (equal); Visualization (equal); Writing – original draft (equal). **T. Stange**: Conceptualization (equal); Data curation (equal); Formal analysis (equal); Investigation (equal); Methodology (equal); Software (equal); Supervision (equal); Validation (equal); Writing – original draft (equal). **L. Krier**: Conceptualization (equal); Data curation (equal); Formal analysis (equal); Investigation (equal); Methodology (equal); Software (equal); Validation (equal); Writing – original draft (equal). **P. Stordiau**: Conceptualization (equal); Data curation (equal); Formal analysis (equal); Investigation (equal); Validation (equal); Writing – original draft (equal). **H. Braune**: Conceptualization (equal); Investigation (equal); Methodology (equal); Supervision (equal); Writing – original draft (equal). **G. Gantenbein**: Conceptualization (equal); Investigation (equal); Methodology (equal); Supervision (equal); Writing – original draft (equal). **J. Jelonnek**: Conceptualization (equal); Project administration (equal); Resources (equal); Supervision (equal); Writing – original draft (equal). **A. Kuleshov**: Conceptualization (equal); Investigation (equal); Methodology (equal); Supervision (equal); Writing – original draft (equal). **H. P. Laqua**: Conceptualization (equal); Investigation (equal); Methodology (equal); Project administration (equal); Supervision (equal); Validation (equal); Writing – original draft (equal). **C. Lechte**: Conceptualization (equal); Investigation (equal); Supervision (equal); Writing – original draft (equal). **S. Marsen**: Conceptualization (equal); Data curation (equal); Investigation (equal); Software (equal); Writing – original draft (equal). **S. K. Nielsen**: Conceptualization (equal); Investigation (equal); Supervision (equal); Writing – original draft (equal). **J. W. Oosterbeek**: Conceptualization (equal); Data curation (equal); Formal analysis (equal); Investigation (equal); Methodology (equal); Software (equal); Supervision (equal); Visualization (equal); Writing – original draft (equal). **B. Plaum**: Conceptualization (equal); Investigation (equal); Methodology (equal); Supervision (equal); Writing – original draft (equal). **R. Ragona**: Conceptualization (equal); Investigation (equal); Software (equal); Validation (equal); Writing – original draft (equal). **J. Rasmussen**: Conceptualization (equal); Methodology (equal); Supervision (equal); Writing – original draft (equal). **T. Ruess**: Conceptualization (equal); Investigation (equal); Methodology (equal); Resources (equal); Writing – original draft (equal). **M. Salewski**: Conceptualization (equal); Methodology (equal); Supervision (equal); Writing – original draft (equal). **M. Thumm**: Conceptualization (equal); Methodology (equal); Supervision (equal); Writing – original draft (equal). **J. Zimmermann**: Data curation (equal); Formal analysis (equal); Investigation (equal); Software (equal); Validation (equal); Writing – original draft (equal).

DATA AVAILABILITY

The data that support the findings of this study are available from the corresponding author upon reasonable request.

REFERENCES

[1] E. E. Salpeter, Phys. Rev. **120**(5), 1528 (1960).
[2] D. Moseev, M. Salewski, M. Garcia-Muñoz, B. Geiger, and M. Nocente, Rev. Mod. Plasma Phys. **2**(1), 7 (2018).
[3] H. Bindslev, J. Atmos. Terr. Phys. **58**(8), 983–989 (1996).
[4] I. Abramovic, A. Pavone, D. Moseev, N. J. Lopes Cardozo, M. Salewski, H. P. Laqua, M. Stejner, T. Stange, S. Marsen, S. K. Nielsen, T. Jensen, and W. Kasparek, W7-X Team, Rev. Sci. Instrum. **90**(2), 023501 (2019).
[5] M. Salewski, F. Meo, M. Stejner, O. Asunta, H. Bindslev, V. Furtula, S. B. Korsholm, T. Kurki-Suonio, F. Leipold, F. Leuterer, P. K. Michelsen, D. Moseev, S. K. Nielsen, J. Stober, G. Tardini, D. Wagner, P. Woskov, and ASDEX Upgrade Team, Nucl. Fusion **50**, 035012 (2010).
[6] J. Rasmussen, S. K. Nielsen, M. Stejner, B. Geiger, M. Salewski, A. S. Jacobsen, S. B. Korsholm, F. Leipold, P. K. Michelsen, D. Moseev, M. Schubert, J. Stober, G. Tardini, and D. Wagner, ASDEX Upgrade Team, Plasma Phys. Controlled Fusion **57**, 075014 (2015).
[7] M. Nishiura, S. Kubo, K. Tanaka, R. Seki, S. Ogasawara, T. Shimozuma, K. Okada, S. Kobayashi, T. Mutoh, K. Kawahata, T. Watari, LHD Experiment Group, T. Saito, Y. Tatematsu, S. B. Korsholm, and M. Salewski, Nucl. Fusion **54**, 023006 (2014).
[8] S. B. Korsholm, A. Chambon, B. Gonçalves, V. Infante, T. Jensen, M. Jessen, E. B. Klinkby, A. W. Larsen, R. Luis, Y. Nietiadi, E. Nonbøl, J. Rasmussen, D. Rechena, M. Salewski, A. Taormina, A. Vale, P. Varela, L. Sanchez, R. M. Ballester, V. Udintsev, and Y. Liu, Rev. Sci. Instrum. **93**(10), 103539 (2022).
[9] M. Salewski, M. Nocente, B. Madsen, I. Abramovic, M. Fitzgerald, G. Gorini, P. C. Hansen, W. W. Heidbrink, A. S. Jacobsen, T. Jensen, V. G. Kiptily, E. B. Klinkby, S. B. Korsholm, T. Kurki-Suonio, A. W. Larsen, F. Leipold, D. Moseev, S. K. Nielsen, S. Pinches, J. Rasmussen, M. Rebai, M. Schneider, A. Shevelev, S. Sipilä, M. Stejner, and M. Tardocchi, Nucl. Fusion **58**, 096019 (2018).
[10] D. Moseev, H. P. Laqua, T. Stange, I. Abramovic, S. K. Nielsen, S. Äkäslompolo, K. Avramidis, H. Braune, G. Gantenbein, S. Illy, J. Jelonnek, J. Jin, W. Kasparek, L. Krier, S. B. Korsholm, C. Lechte, A. Marek, S. Marsen, M. Nishiura, I. Pagonakis, M. Salewski, J. Rasmussen, A. Tancetti, M. Thumm, and R. C. Wolf, W7-X Team, J. Instrum. **15**, C05035 (2020).
[11] V. Erckmann, P. Brand, H. Braune, G. Dammertz, G. Gantenbein, W. Kasparek, H. P. Laqua, H. Maassberg, N. B. Marushchenko, G. Michel, M. Thumm, Y. Turkin, M. Weissgerber, A. Weller, W7-X ECRH Team at IPP Greifswald, W7-X ECRH Team at FZK Karlsruhe, and W7-X ECRH Team at IPF Stuttgart, Fusion Sci. Technol. **52**(2), 291–312 (2007).
[12] H. P. Laqua, K. A. Avramidis, H. Braune, I. Chelis, G. Gantenbein, S. Illy, Z. Ioannidis, J. Jelonnek, J. Jin, L. Krier, C. Lechte, A. Leggieri, F. Legrand, S. Marsen, D. Moseev, H. Oosterbeek, T. Rzesnicki, T. Ruess, T. Stange, M. Thumm, I. Tigelis, and R. C. Wolf, W7-X Team, EPJ Web Conf. **277**, 04003 (2023).
[13] D. Moseev, M. Stejner, T. Stange, I. Abramovic, H. P. Laqua, S. Marsen, N. Schneider, H. Braune, U. Hoefel, W. Kasparek, S. B. Korsholm, C. Lechte, F. Leipold, S. K. Nielsen, M. Salewski, J. Rasmussen, M. Weißgerber, and R. C. Wolf, Rev. Sci. Instrum. **90**(1), 013503 (2019).
[14] A. Tancetti, S. K. Nielsen, J. Rasmussen, D. Moseev, T. Stange, S. Marsen, M. Vecséi, C. Killer, G. A. Wurden, T. Jensen, M. Stejner, G. Anda, D. Dunai, S. Zoletnik, K. Rahbarnia, C. Brandt, H. Thomsen, M. Hirsch, U. Hoefel, N. Chaudhary, V. Winters, P. Kornejew, J. Harris, and H. P. Laqua, W7-X Team, Plasma Phys. Controlled Fusion **65**, 015001 (2023).
[15] J. W. Oosterbeek, N. Chaudhary, M. Hirsch, U. Höfel, and R. C. Wolf, W7-X Team, EPJ Web Conf. **203**, 03010 (2019).
[16] L. Krier, I. Gr. Pagonakis, K. A. Avramidis, G. Gantenbein, S. Illy, J. Jelonnek, J. Jin, H. P. Laqua, A. Marek, D. Moseev, M. Thumm, and W7-X Team, Phys. Plasmas **27**(11), 113107 (2020).
[17] L. Krier, K. A. Avramidis, H. Braune, G. Gantenbein, S. Illy, J. Jelonnek, H. P. Laqua, S. Marsen, D. Moseev, F. Noke, T. Ruess, T. Stange, M. Thumm, and R. C. Wolf, Fusion Eng. Des. **192**, 113828 (2023).
[18] S. Ponomarenko, D. Moseev, T. Stange, T. Windisch, S. Vlasenko, E. Khutoryan, A. Kuleshov, and H. P. Laqua, in *2022 IEEE 2nd Ukrainian Microwave Week (UkrMW), Ukraine, 14–18 November 2022* (IEEE, 2022), pp. 242–245.
[19] I. Bahl, "Monolithic power amplifiers," in *Handbook of RF and Microwave Power Amplifiers*, edited by J. Walker (Cambridge University Press, Cambridge, 2011), pp. 357–410.
[20] S. K. Nielsen, H. Bindslev, L. Porte, J. A. Hoekzema, S. B. Korsholm, F. Leipold, F. Meo, P. K. Michelsen, S. Michelsen, J. W. Oosterbeek, E. L. Tsakadze, G. Van Wassenhove, E. Westerhof, and P. Woskov, Phys. Rev. E **77**, 016407 (2008).

[21] V. Furtula, M. Salewski, F. Leipold, P. K. Michelsen, S. B. Korsholm, F. Meo, D. Moseev, S. K. Nielsen, M. Stejner, and T. Johansen, Rev. Sci. Instrum. **83**(1), 013507 (2012).

[22] P. Tretinnikov, E. Gusakov, and S. Heuraux, Phys. Plasmas **30**(3), 032502 (2023).

[23] P. Woskov, H. Bindslev, F. Leipold, F. Meo, S. K. Nielsen, E. L. Tsakadze, S. B. Korsholm, J. Scholten, C. Tito, E. Westerhof, J. W. Oosterbeek, F. Leuterer, F. Monaco, M. Muenich, and D. Wagner, Rev. Sci. Instrum. **77**(10), 10E524 (2006).

[24] T. H. Lee, *The Design of CMOS Radio-Frequency Integrated Circuits* (Cambridge University Press, Cambridge, 2004), pp. 390–400.

[25] A. Likhachev, S. Ponomarenko, S. Kishko, Yu. Kovshov, V. Zheltov, E. Khutoryan, D. Moseev, T. Stange, and A. Kuleshov, in *2021 22nd International Vacuum Electronics Conference (IVEC), Rotterdam, Netherlands, 27-30 April 2021* (IEEE, 2022), 21740112.

[26] V. Erckmann, W. Kasparek, G. Gantenbein, F. Hollmann, L. Jonitz, F. Noke, F. Purps, M. Weissgerber, W7-X ECRH Teams at IPP Greifswald, FZK Karlsruhe, and IPF Stuttgart, Fusion Sci. Technol. **55**(1), 16–22 (2009).

[27] H. L. Swain and R. M. Cox, Hewlett-Packard J. **34**(4), 23–25 (1983); **27**, 29–34 (1983).

[28] M. V. Kartikeyan, E. Borie, and M. Thumm, *Gyrotrons. High-Power Microwave and Millimeter Wave Technology* (Springer, Berlin, 2004).

[29] T. Stange, W7-X Team, W7-X ECRH Team at KIT, and W7-X ECRH Team at IGVP Stuttgart, "On the path to steady state 10 MW ECRH operation in the operational phase 2 (OP2) of Wendelstein 7-X," in paper presented at the 24th Topical Conference on Radiofrequency Power in Plasmas (TCRFPP), Annapolis, MD, 26–28 September 2022.

[30] L. Krier, K. A. Avramidis, H. Braune, G. Gantenbein, S. Illy, Z. Ioannidis, J. Jelonnek, H. P. Laqua, S. Marsen, D. Moseev, F. Noke, I. Gr. Pagonakis, T. Ruess, T. Rzesnicki, T. Stange, M. Thumm, and R. C. Wolf, in *2021 46th International Conference on Infrared, Millimeter and Terahertz Waves (IRMMW-THz), Chengdu, China, 29 August–3 September 2021* (IEEE, 2021), p. 21388203.

[31] N. Chaudhary, J. W. Oosterbeek, M. Hirsch, U. Hoefel, R. Wolf, and W7-X Team, J. Instrum. **15**, P09024 (2020).

[32] J. W. Oosterbeek, N. Chaudhary, M. Hirsch, M. N. A. Beurskens, U. Höfel, A. Card, M. Marquardt, S. Marsen, M. Stern, and R. C. Wolf, Fusion Eng. Des. **146**(Part A), 959–962 (2019).

[33] N. Chaudhary, M. Hirsch, U. Hoefel, J. W. Oosterbeek, N. Marushchenko, R. Wolf, and W7-X Team, Plasma Phys. Controlled Fusion **64**, 055016 (2022).

[34] M. Hirsch, U. Höfel, J. W. Oosterbeek, N. Chaudhary, J. Geiger, H.-J. Hartfuss, W. Kasparek, N. Marushchenko, B. van Milligen, B. Plaum, T. Stange, J. Svensson, H. Tsuchiya, D. Wagner, G. McWeir, R. Wolf, and W7-X Team, EPJ Web Conf. **203**, 03007 (2019).

[35] Th. Wegner, B. Geiger, R. Foest, A. Jansen van Vuuren, V. R. Winters, C. Biedermann, R. Burhenn, B. Buttenschön, G. Cseh, I. Joda, G. Kocsis, F. Kunkel, A. Quade, J. Schäfer, O. Schmitz, and T. Szepesi, W7-X Team, Rev. Sci. Instrum. **91**(8), 083503 (2020).

[36] H. W. Drawin, Phys. Rep. **37**(2), 125–163 (1978).